

# Single-Phase to Three-Phase Drive System Using Two Parallel Single-Phase Rectifiers

G. MahaboobSubahan<sup>1</sup>

Assistant professor

M.Swetha<sup>2</sup>

Assistant professor

Electrical and Electronics Engineering Department, Annamacharya Institute of Technology & sciences(Autonomous), Rajampet, Andra Pradesh, India

**Abstract**—This paper proposes a single-phase to three-phase drive system composed of two parallel single-phase rectifiers, a three-phase inverter, and an induction motor. The proposed topology permits to reduce the rectifier switch currents, the harmonic distortion at the input converter side, and presents improvements on the fault tolerance characteristics. Even with the increase in the number of switches, the total energy loss of the proposed system may be lower than that of a conventional one. The model of the system is derived, and it is shown that the reduction of circulating current is an important objective in the system design. A suitable control strategy, including the pulse width modulation technique (PWM), is developed. Experimental results are presented as well.

**Index Terms**—Ac-dc-ac power converter, drive system, parallel converter.

## I. INTRODUCTION

Several solutions have been proposed when the objective is to supply a three-phase motors from a single-phase ac mains. It is quite common to have only a single-phase power grid in residential, commercial, and mainly in rural areas, while the adjustable speed drives may request a three-phase power grid.

Single-phase to three-phase ac-dc-ac conversion usually employs a full-bridge topology, which implies in ten power switches, as shown in Fig. 1. This converter is denoted here as conventional topology.

Parallel converters have been used to improve the power capability, reliability, efficiency, and redundancy. Parallel converter techniques can be employed to improve the performance of active power filters, uninterruptible power supplies (UPS), fault tolerance of doubly fed induction generators, and three-phase drives. Usually the operation of converters in parallel requires a transformer for isolation. However, weight, size, and cost associated with the transformer may make such a solution undesirable [20]. When an isolation transformer is not used, the reduction of circulating currents among different converter stages is an important objective in the system design.

In this paper, a single-phase to three-phase drive system composed of two parallel single-phase rectifiers and a three-phase Inverter is proposed, as shown in Fig. 2. The proposed system is conceived to operate where the single-phase utility grid is the unique option available. Compared to the conventional topology, the proposed system permits: to reduce the rectifier switch currents; the total harmonic distortion (THD) of the grid current with same switching frequency or the switching frequency with same THD of the grid current; and to increase the fault tolerance characteristics. In addition, the losses of the proposed system may be lower than that of the conventional counterpart. The aforementioned benefits justify the initial investment of the proposed system, due to the increase of number of switches.

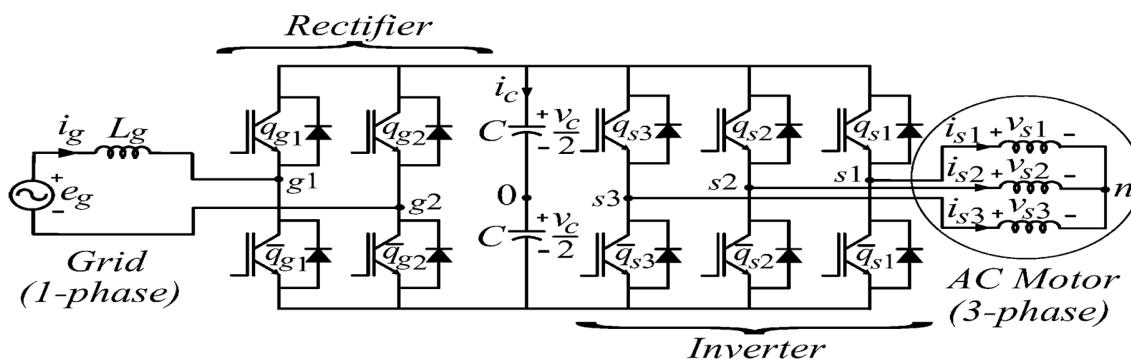


Fig. 1. Conventional single-phase to three-phase drive system

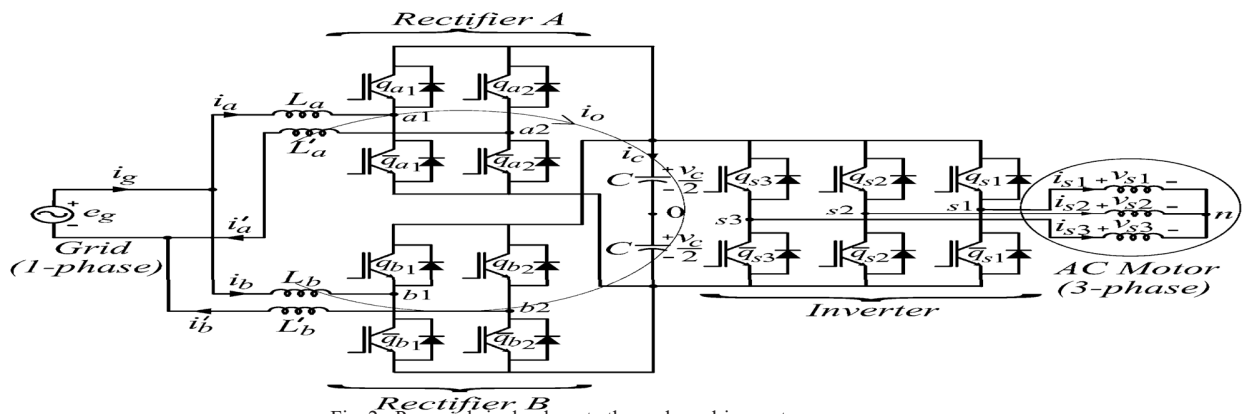


Fig. 2. Proposed single-phase to three-phase drive system

## II PWM STRATEGY

The inverter can be commanded by using an adequate pulsewidth modulation (PWM) strategy for three-phase voltage source inverter (VSI) [19], so that it will not be discussed here. In this section, the PWM strategy for the rectifier will be presented.

The parameter  $\mu$  changes the place of the voltage pulses related to  $v_a$  and  $v_b$ . When  $v_x^* = v_{x\min}^*$  ( $\mu = 0$ ) or  $v_x^* = v_{x\max}^*$  ( $\mu = 1$ ) are selected, the pulses are placed in the begin or in the end of the half period ( $T_s$ ) of the triangular carrier signal [see Fig. 5(a) and (c)]. On the other hand, when  $v_x^* = v_{x\text{ave}}^*$  the pulses are centered in the half period of the carrier signal [see Fig. 5(b) and (d)]. The change of the position of the voltage pulses leads also to the change in the distribution of the zero instantaneous voltages (i.e.,  $v_a = 0$  and  $v_b = 0$ ). With  $\mu = 0$  or  $\mu = 1$  the zero instantaneous voltages are placed at the beginning or at the end of the switching period, respectively, while with  $\mu = 0.5$ , they are distributed equally at the beginning and at the end of the halfperiod. This is similar to the distribution of the zero-voltage vector in the three-phase inverter.

## III. CONTROL STRATEGY

Fig. 3 presents the control block diagram of the system in Fig. 2, highlighting the control of the rectifier. The Rectifier circuit of the proposed system has the same objectives of that in Fig. 1, i.e., to control the dc-link voltage and to guarantee the grid power factor close to one. Additionally, the circulating current  $i_o$  in the rectifier of the proposed system needs to be controlled.

In this way, the dc-link voltage  $v_c$  is adjusted to its reference value  $v_c^*$  using the controller  $R_c$ , which is a standard PI type controller. This controller provides the amplitude of the reference grid current  $I_g^*$ . To control power factor and harmonics in the grid side, the instantaneous reference current  $i_g^*$  must be synchronized with voltage  $e_g$ , as given in the voltage-oriented

(VOC) for three-phase system [32]. This is obtained via blocks  $Ge$ - $ig$ , based on a PLL scheme. The reference currents  $i_a^*$  and  $i_b^*$  are obtained by making  $i_a^* = i_b^* = i_g^*/2$ , which means that each rectifier receives half of the grid current. The control of the rectifier currents is implemented using the controllers indicated by blocks  $R_a$  and  $R_b$ . These controllers can be implemented using linear or nonlinear techniques [33]–[37]. In this paper, the current control law is the same as that used in the two sequences synchronous controller described in [38]. These current controllers define the input reference voltages  $v_a^*$  and  $v_b^*$ . The homopolar current is measured ( $i_o$ ) and compared to its reference ( $i_o^* = 0$ ). The error is the input of PI controller  $R_o$ , that determines the voltage  $v_o^*$ . The calculation of voltage  $v_x^*$  is given from (30) to (32) as a function of  $\mu$ , selected as shown in the Section V. The motor three-phase voltages are supplied from the inverter (VSI). Block VSI-Ctr indicates the inverter and its control. The control system is composed of the PWM command and a torque/flux control strategy (e.g., field-oriented control or volts/hertz control).



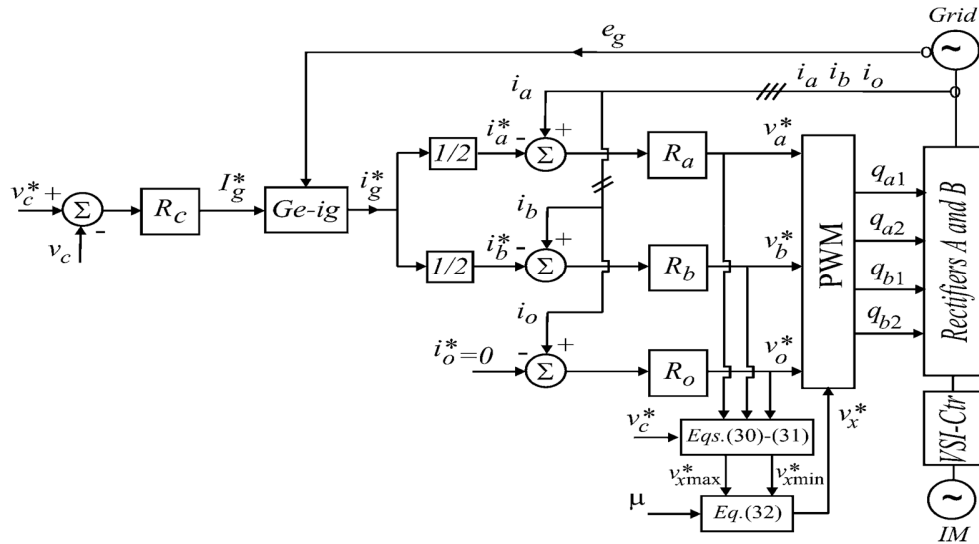


Fig. 3. Control block diagram.

#### IV. HARMONIC DISTORTION

The harmonic distortion of the converter voltages has been evaluated by using the weighted *THD* (*WTHD*). Fig. 4 shows the *WTHD* of voltages generated by rectifiers [ $v_{ab} = (v_a + v_b)/2$  for the proposed configuration and  $v_g = v_{g10} \quad v_{g20}$  for the conventional one] at rated grid voltage as a function of  $\mu$ . Note that the parameter  $\mu$  determines  $v_x^*$  from  $v_c^*$ . The resultant voltage  $v_{ab}$  generated by rectifier is responsible to control  $i_g$  [see (16)], which means that this voltage is used to regulate the harmonic distortion of the utility grid.

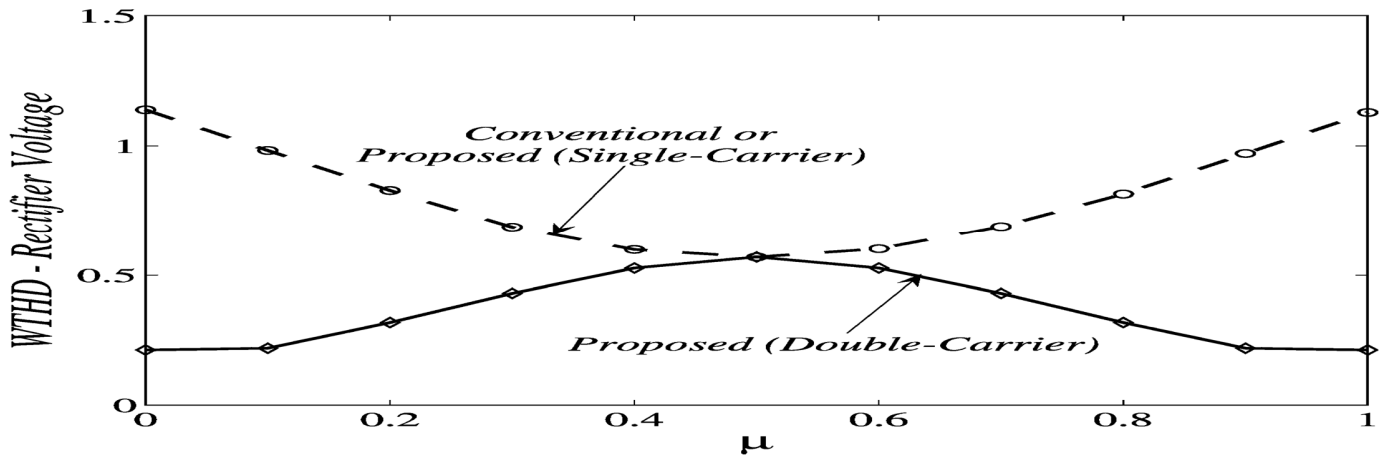


Fig. 4. *WTHD* of rectifier voltage ( $v_{ab}$  for proposed configuration and  $v_g$  for standard configuration) as a function of  $\mu$ .

When the single-carrier PWM is used, the behavior of *WTHD* of the proposed system is similar to that of conventional one for all  $\mu$ , as observed in Fig. 4. When the double-carrier PWM is used with  $\mu = 0.5$ , the *WTHD* is also the same for both configurations. However, for the other values of  $\mu$  the *WTHD* of the proposed system is lower than that of the conventional one. The *WTHD* of the proposed topology (double-carrier with  $\mu = 0$  or  $\mu = 1$ ) is close to 63% of that of the conventional topology (with  $\mu = 0.5$ ). The study has also shown that it is possible to reduce the switching frequency of the proposed system in 60% and still have the same *WTHD* of the standard configuration.

The *WTHD* behavior in Fig. 4 can be explained from Fig. 5. That figure depicts the pole voltages ( $v_{a10}, v_{a20}, v_{b10}, v_{b20}$ ) and their references ( $v_a^*, v_b^*$ ), the triangular carrier signals ( $v_{t1}, v_{t2}$ ), the resultant rectifier voltage ( $v_{ab}$ ) and the circulating voltage ( $v_o$ ). Fig. 5(a) and (c) shows these variables with single-carrier (with  $\mu = 1$ ) and double-carrier (with  $\mu = 1$ ), respectively. For the double-carrier [see Fig. 5(c)] the voltage  $v_{ab}$  has smaller amplitude and better distribution along the half switching period than that of single-carrier [see Fig. 5(a)], which means a lower *WTHD* (as observed in Fig. 4 for  $\mu = 1$ ). On the other hand, for  $\mu = 0.5$  [see Fig. 5(b) and (d)] the distribution of voltage  $v_{ab}$  along the switching period is the same for both cases, i.e., single-carrier and double-carrier have the same *WTHD* (as observed in Fig. 4 for  $\mu = 0.5$ ).

Besides the total harmonic distortion (*THD*) of the grid current  $i_g$ , associated to the *WTHD* of the voltage  $v_{ab}$ , the harmonic distortion analysis must also consider the currents in the rectifiers. This is an important issue due to losses of the converter [39], [40]. The harmonic distortion of the rectifier currents ( $i_a, i_a^d, i_b$ , and  $i_b^d$ ) with double-carrier is higher than that of the grid current  $i_g$ . When the parallel rectifier with double-carrier is used, the *THD* of all these currents are reduced for  $\mu = 0$  or  $\mu = 1$  and increased for  $\mu = 0.5$ . On the other hand, the *THD* of the circulating current is also smaller with  $\mu = 0$  or  $\mu = 1$ . Fig. 6 shows currents  $i_a, i_a^d$ , and  $i_o$  for double-carrier with  $\mu = 1$  and  $\mu = 0.5$ . It can be seen that the mean values of the ripples of all currents are smaller when  $\mu = 1$  is selected. In conclusion,

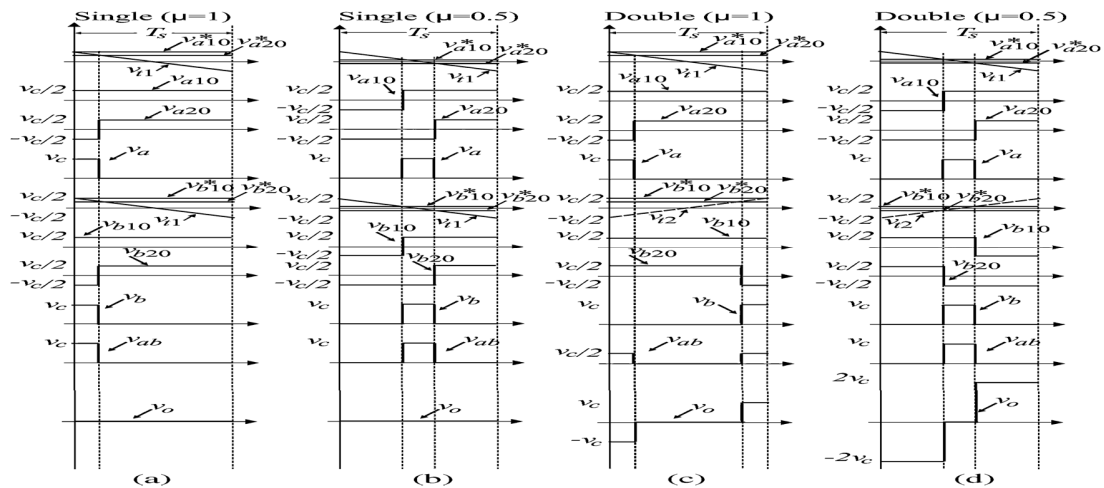


Fig. 5. Variables of rectifiers A and B. (a) Single-carrier with  $\mu = 1$ . (b) Single-carrier with  $\mu = 0.5$ . (c) Double-carrier with  $\mu = 1$ . (d) Double-carrier with  $\mu = 0.5$ .

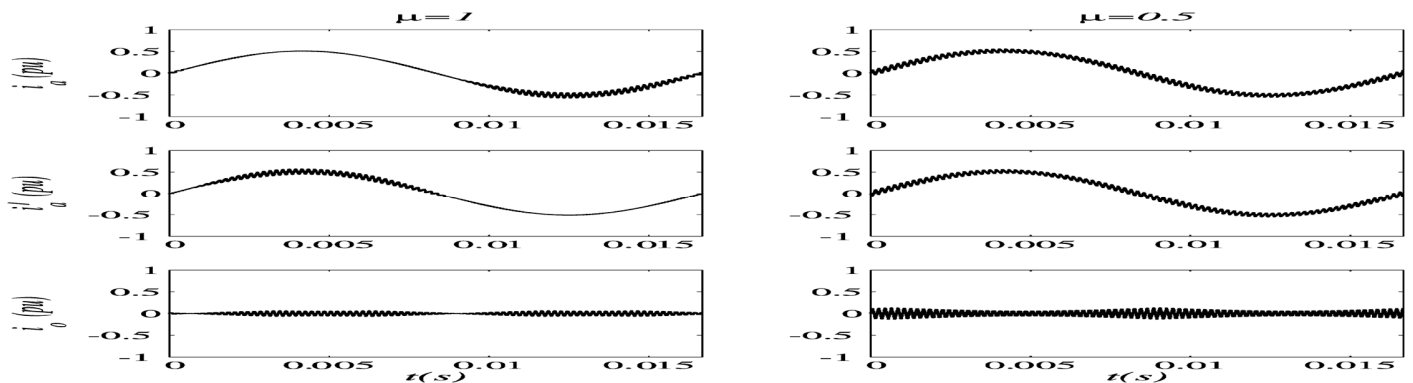


Fig. 6. Currents  $i_a, i_a^d$ , and  $i_o$  for double-carrier with  $\mu = 1$  and  $\mu = 0.5$ .

the optimal rectifier operation is obtained with double-carrier making  $\mu = 0$  or  $\mu = 1$ . A four-carrier approach may also be used. Compared with the two-carrier strategy, the four-carrier strategy permits to reduce the harmonic distortion of the grid current, but increases the rectifier losses.

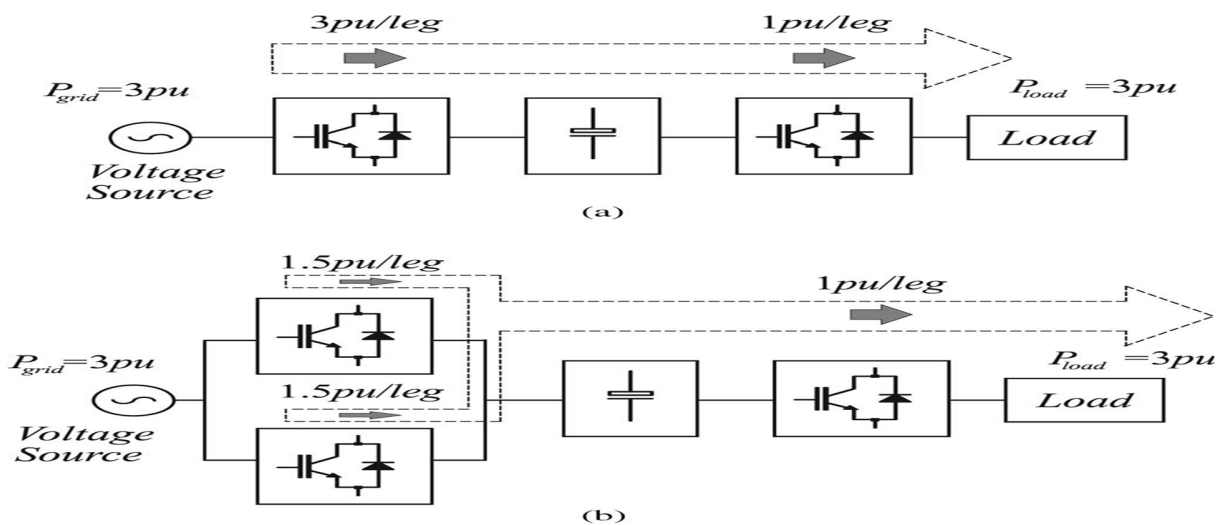


Fig. 7. Flow of active power. (a) Conventional ac–dc–ac single-phase to three- phase converter. (b) Proposed system with two rectifiers.

### V . RATINGS OF SWITCHES

Assuming same rms voltages at both grid and machine sides, a machine power factor of 0.85 and neglecting the converter losses, currents of the rectifier switches normalized in terms of currents of the inverter switches are 2.55 and 1.27 for the conventional and the proposed single-phase to three-phase con- verter, respectively. Fig. 7(a) and (b) shows the flow of active power in the conventional and in the proposed single-phase to three-phase converter, respectively. For balanced system ( $L'_g = L_a = L'_a = L_b = L_b^J$ ), voltage  $v_o$  is close to zero, so that the dc-link voltage is equal to that required by the conventional sys- tem. Since the parallel connection scheme permits to reduce the switch currents and preserve the dc-link voltage, the rating of each power switch in the rectifier side is reduced.

### VI. DC-LINK CAPACITOR

The dc-link capacitor current behavior is examined in this section. Fig. 8 illustrates the harmonic spectrums of the dc-link capacitor current for the conventional converter ( $\mu = 0.5$ ) [see Fig. 8(a)] and for the proposed converter using single-carrier with  $\mu = 0.5$  [see Fig. 8(b)], double-carrier with  $\mu = 0.5$  [see Fig. 8(c)] and double-carrier with  $\mu = 0$  [see Fig. 8(d)]. The proposed converter using double-carrier with  $\mu = 0$  provides the best reduction of the high frequency harmonics. Table I (obtained from Fig. 8) presents the THD of the dc-link capacitor current of the proposed converter ( $THD_p$ ) referred to the THD of the conventional converter ( $THD_c$ ). The highest reduction of THD is obtained for the converter using double-carrier with  $\mu = 0$ . The THD obtained for  $\mu = 1$  is equal to that for  $\mu = 0$ .

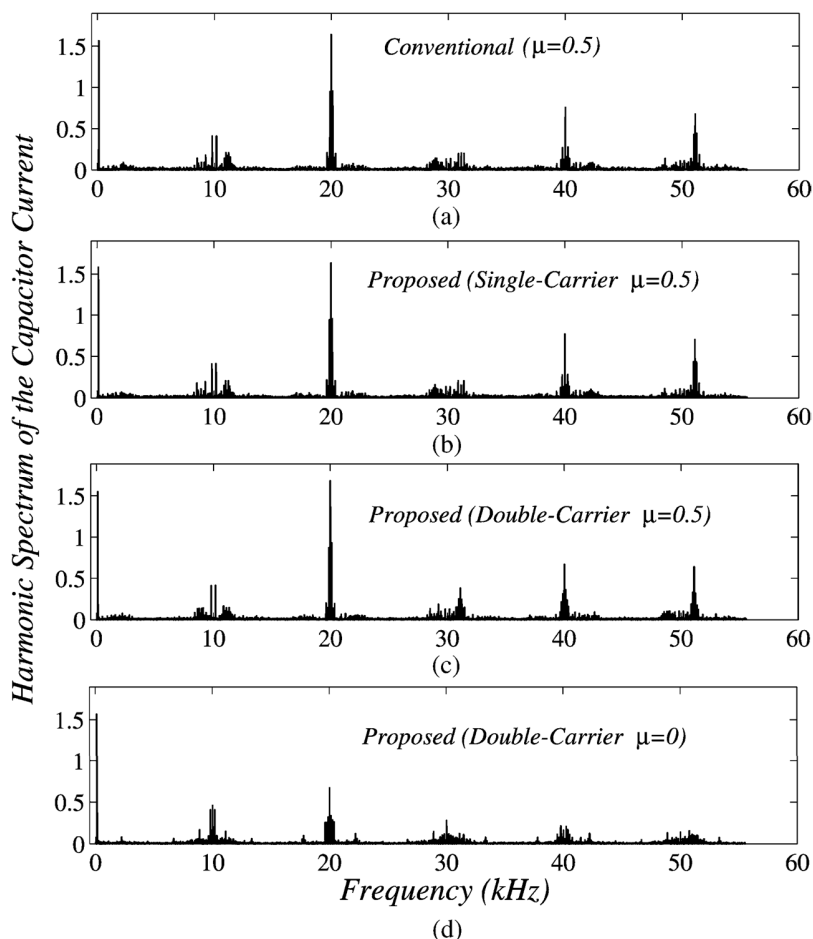


Fig. 8. Harmonic spectrum of the dc-link capacitor current. (a) Conventional converter

TABLE I  
NORMALIZED THD OF DC-LINK CURRENT OF THE PROPOSED CONVERTER

Topology (PWM)	$THD_p/THD_c$
Proposed (Single $\mu = 0.5$ )	0.994
Proposed (Double $\mu = 0.5$ )	1.002
Proposed (Double $\mu = 0$ )	0.717

It is possible to reduce the second order harmonic introduced by single-phase operation, but this is not of interest because it requires unbalancing and increasing rectifier currents  $i_a$  and  $i_b$ .

VII. LOSSES AND EFFICIENCY

The evaluation of the rectifier losses is obtained through regression model. The switch loss model includes: 1) IGBT and diode conduction losses; 2) IGBT turn-ON losses; 3) IGBT turn-OFF losses; and 4) diode turn-OFF energy. The loss evaluation takes into account just the rectifier circuit, since the inverter side of converter is the same for the proposed and standard configurations.

When the rectifiers operate with a switching frequency equal to 5 kHz, the conduction and switching losses of the proposed topology were 70% and 105%, respectively, of the corresponding losses of the conventional topology. Consequently, in this case, the total losses of the proposed topology was smaller than that of the conventional topology. The increase of the switching frequency does not change the conduction losses of both topologies, but increases their switching losses, especially for the proposed topology that has a high number of switches.

The efficiency of the topologies operating with a switching frequency equal to 10 kHz and 5 kHz was evaluated by experimental measurement with a 2 kW load. Table II shows the experimental results of the rectifier efficiency. Such results are obtained for the proposed system ( $\eta_p$ ) normalized in terms conventional one ( $\eta_c$ ), for three cases: 1) both rectifiers operating at 10 kHz and  $L_g = L_g$ ; 2) both rectifiers operating at 10 kHz and  $L_g = L_g/2$ ; and 3) both rectifiers operating at 5 kHz and  $L_g = L_g$ . Three strategies are considered in terms of PWM control: 1) single-carrier with  $\mu = 0.5$  (S-Ca  $\mu = 0.5$ );

VIII .EXPERIMENTAL RESULTS

The system shown in Fig. 2 has been implemented in the laboratory. The setup used in the experimental tests is based on a microcomputer equipped with appropriate plug-in boards and sensors. The system operates with a switching frequency equal to 10 kHz. Steady state, transient, fault analysis, and interleaved operation have been evaluated in the experimental tests.

The steady-state experimental results are shown in Fig. 12. The waveforms in this figure are: (a) voltage and current of the grid, (b) dc-link voltage, (c) currents of rectifier A and circulating current, (d) currents of rectifiers A and B, and (e) load line voltage. Note that, with the proposed configuration, all control demanded for single-phase to three-phase converter has been established. The control guarantees sinusoidal grid current with power factor close to one [see Fig. 12(a)], dc-link and machine voltages under control [see Fig. 12(b) and (e)]. Furthermore, the proposed configuration provides current reduction in the rectifier side (half of the current of the standard topology) [see Fig. 12(d)], which can provide loss reduction. Also, the control guarantees the circulating current close to zero [see Fig. 12(c)].

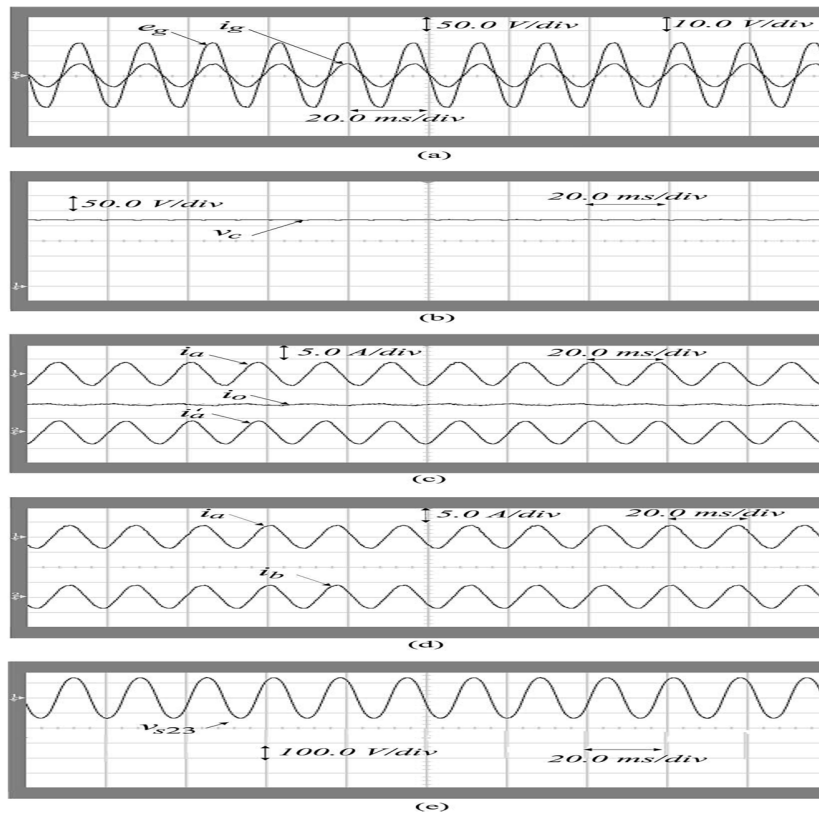


Fig. 12. Steady-state experimental results. (a) Grid voltage ( $e_g$ ) and grid current ( $i_g$ ). (b) Capacitor voltage ( $v_c$ ). (c) Currents of rectifier A ( $i_a$  and  $i_g$ ) and circulating current ( $i_o$ ). (d) Currents of rectifiers A ( $i_a$ ) and B ( $i_b$ ). (e) Line voltage of the load ( $v_{s23}$ ).



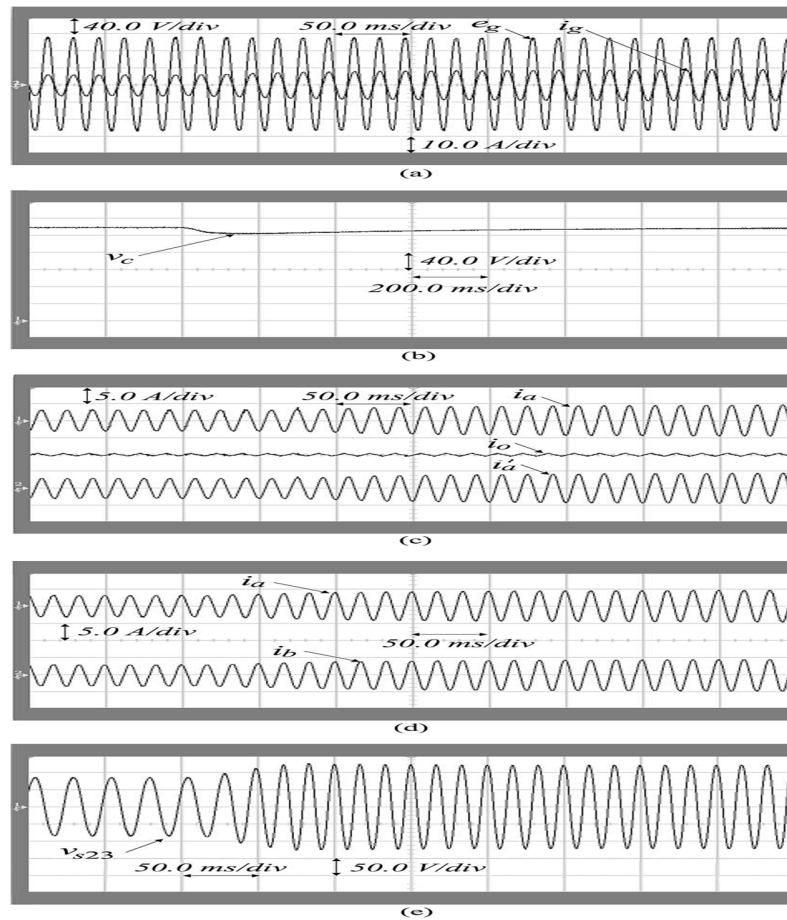


Fig. 13. Experimental results for a volts/hertz transient applied to the three-phase motor. (a) Grid voltage ( $e_g$ ) and grid current ( $i_g$ ). (b) Capacitor voltage ( $v_c$ ). (c) Currents of rectifier A ( $i_o$  and  $i_a$ ) and circulating current ( $i_o$ ). (d) Currents of rectifiers A ( $i_a$ ) and B ( $i_b$ ). (e) Line voltage of the load ( $v_{s23}$ ).

#### IX . CONCLUSION

A single-phase to three-phase drive system composed of two parallel single-phase rectifiers, a three-phase inverter and an induction motor was proposed. The system combines two parallel rectifiers without the use of transformers. The system model and the control strategy, including the PWM technique, have been developed.

The complete comparison between the proposed and standard configurations has been carried out in this paper. Compared to the conventional topology, the proposed system permits to reduce the rectifier switch currents, the THD of the grid current with same switching frequency or the switching frequency with same THD of the grid current and to increase the fault tolerance characteristics. In addition, the losses of the proposed system may be lower than that of the conventional counterpart.

The initial investment of the proposed system (due to high number of semiconductor devices) cannot be considered a drawback, especially considering the scenario where the cited advantages justify such initial investment.

The experimental results have shown that the system is controlled properly, even with transient and occurrence of faults.

## REFERENCES

- [1] P. Enjeti and A. Rahman, "A new single phase to three phase converter with active input current shaping for low cost AC motor drives," *IEEE Trans. Ind. Appl.*, vol. 29, no. 2, pp. 806–813, Jul./Aug. 1993.
- [2] J. Itoh and K. Fujita, "Novel unity power factor circuits using zero-vector control for single-phase input systems," *IEEE Trans. Power Electron.*, vol. 15, no. 1, pp. 36–43, Jan. 2000.
- [3] B. K. Lee, B. Fahimi, and M. Ehsani, "Overview of reduced parts converter topologies for AC motor drives," in *Proc. IEEE PESC*, 2001, pp. 2019–2024.
- [4] C. B. Jacobina, M. B. de R. Correa, A. M. N. Lima, and E. R. C. da Silva, "AC motor drive systems with a reduced switch count converter," *IEEE Trans. Ind. Appl.*, vol. 39, no. 5, pp. 1333–1342, Sep./Oct. 2003.
- [5] R. Q. Machado, S. Buso, and J. A. Pomilio, "A line-interactive single-phase to three-phase converter system," *IEEE Trans. Power Electron.*, vol. 21, no. 6, pp. 1628–1636, May 2006.
- [6] O. Ojo, W. Zhiqiao, G. Dong, and S. Asuri, "High-performance speed- sensorless control of an induction motor drive using a minimalist single-phase PWM converter," *IEEE Trans. Ind. Appl.*, vol. 41, no. 4, pp. 996–1004, Jul./Aug. 2005.
- [7] J. R. Rodríguez, J. W. Dixon, J. R. Espinoza, J. Pontt, and P. Lezana, "PWM regenerative rectifiers: State of the art," *IEEE Trans. Ind. Electron.*, vol. 52, no. 1, pp. 5–22, Feb. 2005.
- [8] M. N. Uddin, T. S. Radwan, and M. A. Rahman, "Fuzzy-logic- controller-based cost-effective four-switch three-phase inverter-fed IPMSynchronous motor drive system," *IEEE Trans. Ind. Appl.*, vol. 42, no. 1, pp. 21–30, Jan./Feb. 2006.
- [9] D.-C. Lee and Y.-S. Kim, "Control of single-phase-to-three-phase AC/DC/AC PWM converters for induction motor drives," *IEEE Trans. Ind. Electron.*, vol. 54, no. 2, pp. 797–804, Apr. 2007.
- [10] L. Woo-Cheol, L. Taeck-Kie, and H. Dong-Seok, "A three-phase parallel active power filter operating with PCC voltage compensation with consideration for an unbalanced load," *IEEE Trans. Power Electron.*, vol. 17, no. 5, pp. 807–814, Sep. 2002.
- [11] L. Asiminoaei, C. Lascu, F. Blaabjerg, and I. Boldea, "Performance improvement of shunt active power filter with dual parallel topology," *IEEE Trans. Power Electron.*, vol. 22, no. 1, pp. 247–259, Jan. 2007.
- [12] L. Asiminoaei, E. Aeloiza, P. N. Enjeti, F. Blaabjerg, and G. Danfoss, "Shunt active-power-filter topology based on parallel interleaved inverters," *IEEE Trans. Ind. Electron.*, vol. 55, no. 3, pp. 1175–1189, Mar. 2008.
- [13] T. A. Chaer, J.-P. Gaubert, L. Rambault, and M. Najjar, "Linear feedback control of a parallel active harmonic conditioner in power systems," *IEEE Trans. Power Electron.*, vol. 24, no. 3, pp. 641–653, Mar. 2009.
- [14] M. Ashari, W. L. Keerthipala, and C. V. Nayar, "A single phase parallelly connected uninterruptible power supply/demand side management system," *IEEE Trans. Energy Convers.*, vol. 15, no. 1, pp. 97–102, Mar. 2000.
- [15] M. Pascual, G. Garcera, E. Figueres, and F. Gonzalez-Espin, "Robust model-following control of parallel UPS single-phase inverters," *IEEE Trans. Ind. Electron.*, vol. 55, no. 8, pp. 2870–2883, Aug. 2008.
- [16] J. Guerrero, J. Vasquez, J. Matas, M. Castilla, and L. de Vicuna, "Control strategy for flexible microgrid based on parallel line-interactive UPS systems," *IEEE Trans. Ind. Electron.*, vol. 56, no. 3, pp. 726–736, Mar. 2009.
- [17] P. Flannery and G. Venkataramanan, "A fault tolerant doubly fed induction generator wind turbine using a parallel grid side rectifier and series grid side converter," *IEEE Trans. Power Electron.*, vol. 23, no. 3, pp. 1126–1135, May 2008.
- [18] R. M. Cuzner, D. J. Nowak, A. Bendre, G. Oriti, and A. L. Julian, "Mitigating circulating common-mode currents between parallel soft-switched drive systems," *IEEE Trans. Ind. Appl.*, vol. 43, no. 5, pp. 1284–1294, Sep./Oct. 2007.
- [19] C. B. Jacobina, E. C. dos Santos Jr., E. R. C. da Silva, M. B. R. Correa, A. M. N. Lima, and T. M. Oliveira, "Reduced switch count multiple three-phase ac machine drive systems," *IEEE Trans. Power Electron.*, vol. 23, no. 2, pp. 966–976, Mar. 2008.
- [20] J.-K. Park, J.-M. Kwon, E.-H. Kim, and B.-H. Kwon, "High-performance transformerless online UPS," *IEEE Trans. Ind. Electron.*, vol. 55, no. 8, pp. 2943–2953, Aug. 2008.